



CHORUS

This is the accepted manuscript made available via CHORUS. The article has been published as:

Combined influence of hydrodynamics and chemotaxis in the distribution of microorganisms around spherical nutrient sources

Nikhil Desai and Arezoo M. Ardekani

Phys. Rev. E **98**, 012419 — Published 31 July 2018

DOI: [10.1103/PhysRevE.98.012419](https://doi.org/10.1103/PhysRevE.98.012419)

Combined influence of hydrodynamics and chemotaxis in the distribution of microorganisms around spherical nutrient sources

Nikhil Desai and Arezoo M. Ardekani*
*School of Mechanical Engineering, Purdue University,
West Lafayette, Indiana, USA, 47907.*

(Dated: July 5, 2018)

We study how the interaction between hydrodynamics and chemotaxis affects the colonization of nutrient sources by microorganisms. We use an individual based model and perform probabilistic simulations to ascertain the impact of important environmental and motility characteristics on the spatial distribution of microorganisms around a spherical nutrient source. In general, we unveil four distinct regimes based on the bulk distribution of the microorganism positions: (i) strong surface colonization, (ii) rotary diffusion induced ‘off-surface’ accumulation, (iii) a depletion zone in the spatial distribution, and, (iv) no appreciable aggregation; with their occurrence being contingent on the relative strengths of hydrodynamic and chemotactic effects. More specifically, we show that the extent of surface colonization first increases, then reaches a plateau and finally decreases as the nutrient availability is increased. We also show that surface colonization reduces monotonically as the mean run-length of the chemotactic microorganisms increases. Our study provides an insight onto the interplay of two important mechanisms governing microorganism behavior near nutrient sources, isolates each of their effects, and thus offers greater predictability of this non-trivial phenomenon.

I. INTRODUCTION

Chemotaxis can be defined as the ability of bacteria to perceive gradients in ambient nutrient/chemical concentrations and adjust their motility so as to ‘climb’ up or down these gradients. It is one of the most widely studied properties of bacteria, particularly for the enteric bacterium *E. coli* [1–4]. The chemical responsible for chemotaxis is called the chemoeffector. The motion of *E. coli* is termed ‘run-and-tumble’ because it consists of almost straight runs separated by sudden tumbles, i.e., abrupt changes in the swimming direction [1–4]. Bacteria rely on temporal comparison of ambient nutrient concentrations to gauge chemoeffector gradients, and refine their motion as required [5–9]. Based on the feedback, a variety of changes can take place to alter bacterial motion, e.g., a change in swimming speed as a function of ambient concentration (chemokinesis), a change in the frequency of tumbling, or even a shift in the regime of swimming from run-and-tumble to ‘run-reverse-and-flick’ [10]. The cumulative effect of the above sequence of actions is to prolong the bacterium’s stay in any desired region. For example, chemokinesis can either slow bacteria down in regions of high nutrient concentration, or it can speed them up so as to have proportionately faster gradient-climbing. Similarly, bacteria are known to increase their average exposure to nutrients and thus fulfill their energetic requirements, by tumbling (or reversing) less often in nutrient hot-spots. In addition to chemotaxis—which is an ‘active response’ by a bacterium to ambient physico-chemical stimuli—a bacterium’s motility can also get altered ‘passively’ via hydrodynamic interactions (H.I.)

with nearby boundaries [11]. Some examples are “swimming on the right-hand side” [12], “swimming in circles” [13–17], reversal of swimming direction [18] and wall-attraction/accumulation [19–26]. These near surface phenomena, coupled with bacterial chemotaxis, are of utmost importance in the comprehension of bio-film formation and evolution [27–29]. While studies focusing solely on H.I. (ref. [12]–[26]), on chemotaxis without H.I. [30–38], or on chemotaxis and H.I. due to self-generated bacterial flows in infinite domains [39, 40] abound; the combined effect of chemotaxis and H.I. on the locomotion of microorganisms near a boundary that is also a source of a chemoattractant, has not been studied in detail. The studies that do consider the effects of fluid flow on bacterial motion (chemotactic or otherwise) near surfaces have been mostly limited to the cases where the bacterial cell is translated and rotated by a pre-existing background flow [31–36]. In absence of any background flows, a consistent description of H.I.s should involve fluid-flow that is generated on account of bacterial swimming and its proximity to surfaces.

In this paper, we aim to understand the combined/competitive effects of hydrodynamic and chemotactic attraction of model microorganisms to spherical nutrient sources. We study the motion of a bacterium that can run-and-tumble, near a stationary, spherical surface which acts as a source of the chemoeffector. Therefore, the motion is dictated by three different mechanisms: (i) translation due to inherent motility as well as hydrodynamic interaction (attraction) with the nutrient source (which can be a rigid sphere or a drop), (ii) rotation due to hydrodynamic interaction and random effects like thermal/athermal diffusion, and, (iii) chemotactic re-orientation due to the spatial distribution of a chemoeffector having a prescribed concentration on the surface of the source [30].

* ardekani@purdue.edu

The fluid flow far from a bacterium can be modeled as that due to a force dipole, i.e., two equal and opposite, collinear forces with an infinitesimal separation between them [24]. A force dipole that lies within a few (1-3) swimmer body lengths from the surface of a rigid sphere (which, in an experiment, can be a colloid [41] or an isolated nutrient source like a marine snow particle) is prone to getting ‘hydrodynamically trapped’ onto the surface of the sphere [25, 26]. Beyond this separation, hydrodynamics alone cannot lead to attachment of microorganisms onto nutrient sources. In fact, Drescher *et al.* performed experiments and concluded that hydrodynamics becomes important only when a bacterium reaches “within a few microns” from a surface, and that hydrodynamic interactions successfully explain the “long residence times” of *E. coli* near no-slip surfaces [42]. This means that in order for hydrodynamics-based capture to occur, a bacterium must reach within an $O(1)$ body length from the spherical surface. This ‘initial approach’ could either be a chance encounter, or directed motion in the form of chemotaxis. It is this idea that motivates our study to understand how effective chemotaxis is, in conjunction with hydrodynamics, in the ‘capture’ of microorganisms around a spherical nutrient source with prescribed surface concentration of the chemoattractant.

A study of this type has been carried out in the past by Jackson [30], but without accounting for any hydrodynamic interactions. Another related work is by Bearon [35] where they quantify the rate at which motile bacteria colonize sinking aggregates like marine snow, phytoplankton, etc [38]. This study neglects H.I.s and considers the effect of the background flow (generated due to a sphere settling at zero Reynolds number [43]) on the bacterium’s position and orientation, but does not consider biased tumbling due to chemotaxis. In a similar fashion, Locsei and Pedley [36], studied the motion of a bacterium tracking an alga wherein they evaluate a background flow field due to a model algal cell. They then use this flow to translate and rotate the bacterial cell, much like Bearon, and specifically neglect other H.I.s between the algal and the bacterial cell. In addition, they model chemotaxis in an empirical fashion based on experimental observations [44]; where the chemotactic re-orientation involves just a reversal in the swimmer direction whenever the separation between the algal and bacterial cells exceeds a threshold.

In this paper, we wish to provide a mathematical model that consistently accounts for chemotaxis and hydrodynamic interactions, in situations where no other background flow exists. Towards this, it is essential to include, (i) chemotactic bias in bacterial motion stemming from the temporal comparison of nutrient concentrations by a bacterium, and, (ii) the fluid-flow (and concomitant bacterial motion) that stems solely from the interaction between the bacterium and the solid surface/boundary. Our objective is to obtain the spatial distribution (in the form of a probability distribution function, or, p.d.f.) of non-interacting chemotactic swimmers ‘released’ at a

given separation from the (nutrient) source, and with an arbitrary initial orientation. This p.d.f. will, in general, be a function of: (i) hydrodynamic parameters like the size (diameter) of the source, the swimming speed of the microorganism and the thrust force it exerts on the fluid, i.e., its dipole strength; and, (ii) chemotactic parameters like the chemoeffector concentration on the surface of the source and the tumbling frequency of the microorganism. A thorough understanding of these functional dependencies is warranted to successfully isolate the effects of chemotaxis from those of hydrodynamics; and in the process, better understand the dynamics of microorganism locomotion and colonization in the context of lab-on-a-chip setups or marine ecosystems.

The rest of the paper is organized as follows. We first describe the governing equations of fluid flow and the boundary conditions on the surface of a rigid, stationary sphere (which, in our case, represents the source of chemoattractant). This enables us to discuss the hydrodynamics induced locomotion of the model swimmer. We then describe the randomness in the swimmer motion, the chemoattractant distribution and the modeling of run-and-tumble chemotaxis for a single microswimmer. We also comment on the near field effects and how they are expected to alter our model. Once the mathematical model is laid out, we present the results of the probabilistic simulations for the translational and rotational dynamics of the swimmer. In all cases, we perform relevant comparative studies and discussion of the results, to pinpoint the influence of different parameters involved. Finally, we end by making some concluding remarks.

II. MATHEMATICAL MODELING & METHODOLOGY

A. Hydrodynamic Interaction

The contribution of the microorganism to the fluid flow is modeled as a pusher force dipole (dipole strength F oriented along \mathbf{p} ; see Fig. 1). Even though the force dipole representation is most accurate when the flow field is being analyzed far away from the microorganism, we note that such representations have been shown to be accurate at distances as small as a few body lengths away from rigid walls [19, 24], and interfaces [45, 46]. These have also been used to study the locomotion, and hydrodynamic trapping, of microswimmers around rigid spherical obstacles [25] and spherical drops [26]. To model the bacterial motion in the unbounded case (when it is far away from any surface), we make two additions: (i) we allow the force dipole to have swimming velocity $V_s \mathbf{p}$ in an unbounded fluid, where V_s is the swimming speed of the microorganism; (ii) we assume that in an unbounded fluid, the dipole orientation can ‘tumble’ with a characteristic tumbling frequency τ_0^{-1} and diffuse over the unit sphere with a (rotary) diffusivity D_r , this part is discussed in detail in Section II B.

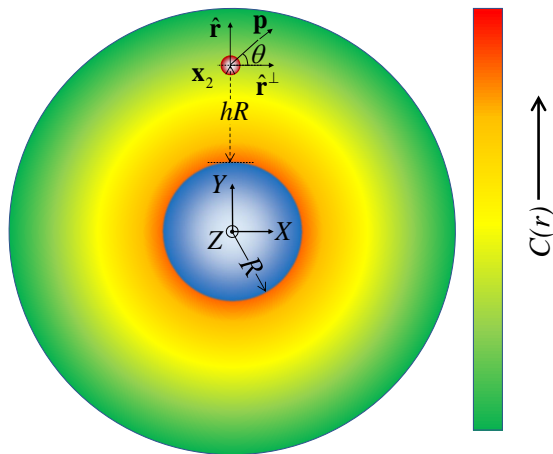


FIG. 1. (Color online) A schematic of the problem being solved, showing a spherical nutrient source of radius R , a spherical swimmer of radius b oriented along the unit vector \mathbf{p} , and the spherically symmetric chemoattractant distribution around it $C(r)$. The origin of a ‘fixed’ coordinate system XYZ lies at the center of the source. The coordinate system defined by the unit vectors $\hat{\mathbf{r}}$, $\hat{\mathbf{r}}^\perp$ and $\hat{\mathbf{r}}^\perp \times \hat{\mathbf{r}}$ can rotate and translate with respect to the fixed coordinate system, as the swimmer moves through the fluid. In a quiescent, unbounded, fluid ($h \rightarrow \infty$), the swimmer will swim along the direction \mathbf{p} . The hydrodynamic interaction induced translational velocity, \mathbf{u}_{HI} , and rotational velocity, $\boldsymbol{\Omega}_{HI}$, of the swimmer is expressed as a function of the swimmer separation from the surface h , and its in-plane orientation θ (see equations 4 and 5). Note that h is the dimensionless separation of the swimmer from the source.

The effect of a solid boundary near the bacterium, i.e., the hydrodynamic interaction (H.I.), is incorporated by first solving the governing equations for fluid-flow with appropriate boundary conditions. These include the differential forms of the conservation of mass,

$$\nabla \cdot \mathbf{v} = 0, \quad (1)$$

and momentum,

$$-\nabla p + \mu \nabla^2 \mathbf{v} = -F (\mathbf{p} \cdot \nabla) \{\mathbf{p} \cdot \delta(\mathbf{x} - \mathbf{x}_2)\}, \quad (2)$$

in the Stokes flow regime, because for the length scales involved in our problem, the flow inertia is negligible. Equations 1 and 2 need to be solved subject to the boundary conditions:

$$\begin{aligned} \mathbf{v}(|\mathbf{x}| = R) &= 0, \\ \mathbf{v}(|\mathbf{x}| \rightarrow \infty) &= 0 \end{aligned} \quad (3)$$

In the above equations, \mathbf{v} , p and μ are the fluid’s velocity, pressure and dynamic viscosity, respectively. R is the radius of the spherical nutrient source. \mathbf{x} is the position at which the velocity needs to be evaluated, \mathbf{x}_2 is the position vector from the origin of the coordinate system to the center of the microorganism (see Fig. 1), and $\delta(\mathbf{x})$ is the three-dimensional Dirac-delta function.

Equations 1 - 3 can be solved for $\mathbf{v}(\mathbf{x})$ and $p(\mathbf{x})$, by using the method of images as shown in ref. [47]. Thereafter, an application of the Faxen’s law for a sphere, by treating the image flow field as an ambient flow and utilizing the force free and torque free conditions, yields the linear (\mathbf{u}_{HI}) and angular ($\boldsymbol{\Omega}_{HI}$) velocity of the force dipole, due to the hydrodynamic influence of the nearby particle (see ref. [25, 26]):

$$\begin{aligned} \frac{\mathbf{u}_{HI}}{V_s} &= -\frac{3A\alpha_D(1-3\sin^2\theta)(A+h)}{2h^2(2A+h)^2} \hat{\mathbf{r}} \\ &+ \frac{3A^3\alpha_D(2A^2+6Ah+3h^2)\sin 2\theta}{4h^2(2A+h)^2(A+h)^3} \hat{\mathbf{r}}^\perp, \end{aligned} \quad (4)$$

$$\frac{\boldsymbol{\Omega}_{HI}}{V_s/b} = -\frac{3A^3\alpha_D(2A^2+6Ah+3h^2)\sin 2\theta}{4h^3(2A+h)^3(A+h)^2} (\hat{\mathbf{r}}^\perp \times \hat{\mathbf{r}}). \quad (5)$$

In equations 4 and 5, b is a measure of the swimmer size (if the swimmer is assumed to be spherical, then b is its radius), $h = (|\mathbf{x}_2| - R)/b$ is the dimensionless separation of the microswimmer from the surface of the source, $A = R/b$ is the dimensionless radius of the source, θ is the in-plane orientation of the microswimmer (see Fig. 1), and $\alpha_D = F/(8\pi\mu b^2 V_s)$ is the dimensionless dipole strength of the microswimmer. Before proceeding, we make an important note regarding the generality of the hydrodynamic aspect of our study. Equations 4 and 5 describe the swimming dynamics of a model microorganism near a rigid spherical nutrient source. It is also possible to derive the same for motion around spherical drops by using appropriate boundary conditions in place of 3, as done by Shaik and Ardekani [48]. In this study, we restrict ourselves to the analysis of motion around rigid, spherical nutrient sources (e.g., marine snow particles). However, a similar analysis can be performed for a nutrient source like an oil drop (i.e., for a spherical fluid-fluid interface); for details see ref. [26] and the Appendix. For a viscosity ratio corresponding to crude oil, there is only a minor quantitative change in the final results of interest (see Fig. 12 in the Appendix). Therefore, we note that our study also reflects the accumulation trends around crude oil drops that are the sole source of carbon for a wide class of marine bacteria [49].

Once \mathbf{u}_{HI} and $\boldsymbol{\Omega}_{HI}$ are known, the motion of the swimmer can be defined in terms of the evolution equations for its position \mathbf{x}_2 and orientation \mathbf{p} . The former is given by,

$$\frac{d\mathbf{x}_2}{dt} = \mathbf{u}_{HI} + V_s \mathbf{p}, \quad (6)$$

while the *hydrodynamic component* of the latter is,

$$\left. \frac{d\mathbf{p}}{dt} \right|_{\text{hydrodynamic}} = \boldsymbol{\Omega}_{HI} \times \mathbf{p}. \quad (7)$$

Equation 7 is not complete yet because we haven’t accounted for two important randomness effects in the motion of any bacterium: the run-and-tumble motion and

thermal/athermal diffusion. We now turn our attention to modeling these effects.

B. Chemotactic Re-orientation

The motion of a bacterium in an unbounded, quiescent fluid is characterized by run-and-tumble, i.e., nearly straight swimming (runs) interspersed with abrupt re-orientations (tumbles) due to certain flagellar mechanisms [50–52]. The runs themselves are not perfectly straight due to various reasons (Brownian rotation, flagellar imperfections, ATP availability) and the bacterium is seen to undergo rotary diffusion during the course of each run [53]. In this Section, we discuss the incorporation and implementation of these re-orientations into our model. The rotary diffusion is straightforward and just adds a random component to the right-hand-side of equation 7; written as a stochastic differential equation, this yields:

$$\mathbf{p}_{n+1} = \mathbf{p}_n + \Delta t (\boldsymbol{\Omega}_{HI})_n \times \mathbf{p}_n + \sqrt{4D_r \Delta t} \boldsymbol{\eta}_r \times \mathbf{p}_n, \quad (8)$$

where D_r is the rotary diffusivity of the bacterium and $\boldsymbol{\eta}_r$ is the Gaussian white noise on the unit sphere [3, 53, 54]. In general, the rotary diffusivity is obtained by using the Stokes-Einstein relations along with the mobility matrices of the system under consideration [11]. Due to the changing geometry of the problem, the mobility matrices will be a function of the position and the orientation of the microorganism, and the effect of Brownian rotation will be a more involved stochastic differential equation (see ref. [55, 56] for details) instead of eqn. 8. Also, the magnitude of the fluctuations will be a function of the microorganism's distance from the source. For the sake of simplicity however, we assume the mobility matrix to be constant and isotropic, in which case eqn. 8 holds. We emphasize that this does not alter the essential physics that we observe in our study. We discuss this idea in detail in the Appendix. The tumbling of the bacterial cell is a probabilistic event, modeled as a Poisson process with rate τ_0^{-1} [3]. This means that in an unbounded fluid, the probability of a tumble to occur after an infinitesimal interval dt is constant and is given by,

$$P_{t,0} = dt/\tau_0. \quad (9)$$

Therefore, $1/\tau_0$ is the mean tumbling frequency for a bacterium, and a tumble is effected by the following ‘rule’ [57, 58]:

$$\begin{aligned} \mathbf{p}_{n+1} &= \phi \mathbf{p}_n + (1 - \phi) \mathbf{p}', \\ \phi &\equiv H(\mathfrak{R}_{n+1} - P_{t,0}), \end{aligned} \quad (10)$$

where H is the Heaviside function [59], and \mathfrak{R}_{n+1} is a random number chosen from a uniform distribution. Therefore, during a run (if $P_{t,0} < \mathfrak{R}_{n+1}$), the bacterium re-orientates ‘smoothly’ via equation 8, but in case of a tumble (if $P_{t,0} > \mathfrak{R}_{n+1}$) it changes its orientation instantaneously

to a new orientation \mathbf{p}' . This post-tumble orientation could either be one from a uniform distribution on the unit sphere (an isotropic tumble); or, it could be biased, i.e., correlated in some way to the pre-tumble orientation (anisotropic tumble). In this study, we use a probability distribution $g(\beta)$, of the angle β between the pre- and post-tumble orientations which has been observed experimentally for the bacterium *E. coli* [1], and a succinct mathematical expression is provided in ref. [60]: $g(\beta) = (1 + \cos \beta)/2$. Note that in reality, a tumble is not instantaneous (it takes around 0.1s) but we assume it to be so for the current work.

The run-and-tumble described thus far enables a bacterium to perform a ‘random walk’ through its environment, just like Brownian/diffusive motion. The effective diffusivity of this random walk is given by $D_{eff} = V_s^2 \tau_0/3$ [61]. The true utility of this motility feature however, is observed when a bacterium forages for nutrients. An intricate mechanism [22, 52] allows the bacterium to alter its tumbling frequency—or equivalently, its run time—in such a way that it spends more (resp. less) time in a desired (resp. undesired) region, e.g., in a region that is rich (resp. poor) in nutrients. As a result, the rate of the Poisson process (or, equivalently, the tumbling frequency) is no longer a constant τ_0^{-1} , but it changes depending on the nutrient exposure of the bacterium. If the organism finds itself in regions of progressively increasing nutrient concentration, then its tumbling frequency reduces ($\tau > \tau_0$); and if the organism moves to regions of declining nutrient concentrations, then the tumbling frequency stays unaltered at $\tau = \tau_0$. It is therefore imperative to have an idea about the nutrient distribution, before proceeding on to model bacterial chemotaxis. The concentration C of the nutrient/chemoeffector is governed by the following conservation equation:

$$\frac{\partial C}{\partial t} + \nabla \cdot (C\mathbf{u}) = D_C \nabla^2 C, \quad (11)$$

subject to the boundary conditions:

$$\begin{aligned} C(|\mathbf{x}| = R) &= C_0, \\ C(|\mathbf{x}| \rightarrow \infty) &= 0. \end{aligned} \quad (12)$$

D_C in eqn. 11 is the nutrient diffusivity. We now proceed to make two simplifications to equation 11. Firstly, we consider steady-state nutrient distribution, thus dropping the first term on the left hand side of equation 11. Next, we note that the characteristic Peclet number for the problem is very small, which allows us to neglect the advection terms in eqn. 11. The Peclet number is,

$$\text{Pe} = \frac{V_s l_{ref}}{D_C}, \quad (13)$$

where $V_s \approx 10 \mu\text{m/s}$ is the reference velocity scale (the bacterium's swimming speed) and l_{ref} is a reference length scale (for phytoplankton, $l_{ref} \approx 10 \mu\text{m}$; for oil drops, $l_{ref} \approx 20 - 60 \mu\text{m}$ [63–65]). The value of D_C for some typical nutrients—like C_6 sugar, or hydrocarbons

like CH_4 —is $\approx 10^{-5}$ cm^2/s [66, 67]. For the above mentioned parameters, we see that the Pe is $O(0.1)$, and thus advection can be neglected as a first approximation. As a result, we obtain the very simple diffusion equation for the chemoeffector concentration,

$$D_C \nabla^2 C = 0, \quad (14)$$

which can be solved using the boundary conditions 12 to get:

$$C(r) = \frac{C_0 R}{r}, \quad (15)$$

here $r = |\mathbf{x}_2|$ is the radial distance from the origin of the coordinate system (see Fig. 1). We can now define the chemotactic motion of the bacterium by relating its tumbling frequency to the temporal evolution of the nutrient concentration C in the bacterial reference frame. Towards this, we employ the ‘bi-phasic tumbling frequency’ model developed by Brown and Berg for *E. coli* [2], but without the ‘memory effect’, i.e.,

$$\tau = \begin{cases} \tau_0 \exp\left(\alpha_C \frac{K_D}{(K_D + C)^2} \frac{DC}{Dt}\right), & \frac{DC}{Dt} > 0 \\ \tau_0, & \frac{DC}{Dt} \leq 0 \end{cases} \quad (16)$$

where K_D is a measure of how well the chemoattractant binds to the chemoreceptor, and α_C is a time scale characteristic to the system being studied. A lack of the ‘memory effect’ means that τ depends only on the *instantaneous* rate of change/material derivative of C (i.e., DC/Dt) with respect to the bacterial motion, and not on the averaged time history of nutrient concentration [68]. It is clear that if the material derivative is positive, then the run-time $\tau > \tau_0$; if the material derivative is negative, then the run-time does not change, as observed in experiments with *E. coli* [2]. Equation 16 thus provides us

with a framework that explains how tumbles assist a microorganism in foraging for desired chemical species. As the organism swims through its environment, it ‘senses’ the changes in the ambient nutrient concentration and alters its tumbling statistics according to equation 16 [69, 70]. Therefore, in the presence of a chemoeffector, a tumble occurs within an infinitesimal time interval dt , if $P_t = dt/\tau > \mathfrak{R}_{n+1}$; notice how P_t can be lesser than $P_{t,0}$ (equation 9) if a chemoeffector is involved. We note that although the above model was developed for the enteric *E. coli*, a judicious choice of the quantity α_C and slight changes in the type of re-orientation can enable us to mimic chemotactic responses that are not of the ‘run-and-tumble’ type, e.g., see the recent work by Son *et al.* [71].

C. Near wall Effects

So far, we have described the effect of H.I. and chemotaxis on the locomotion of a microorganism modelled as a force dipole. These descriptions are apt in situations when the swimmer is a few (> 2) body-lengths away from the source. What happens when the swimmer drifts to within 2 body lengths from the solid surface? In such a scenario, the far field force dipole assumption can lead to the swimmer ‘penetrating’ into the solid surface; an occurrence which is clearly aphysical. This could be prevented by: (i) the inclusion of higher order singularities (and images) in equation 2; or (ii) use of the lubrication/thin-film approximation, as the swimmer-surface distance becomes very small. Both these methods are unwieldy, and so, for the sake of simplicity, we model the ‘near field’ hydrodynamics as a hardcore repulsion[20, 21, 25], i.e., we set the normal velocity of the swimmer to be zero if the swimmer distance becomes less than 1 body-length from the surface:

$$\frac{d\mathbf{x}_2}{dt} = \begin{cases} \mathbf{u}_{HI} + V_s \mathbf{p}; & |\mathbf{x}_2| \leq (R + b), (\mathbf{u}_{HI} + V_s \mathbf{p}) \cdot \hat{\mathbf{r}} > 0 \\ (\mathbf{u}_{HI} + V_s \mathbf{p}) \cdot \hat{\mathbf{r}}^\perp; & |\mathbf{x}_2| \leq (R + b), (\mathbf{u}_{HI} + V_s \mathbf{p}) \cdot \hat{\mathbf{r}} \leq 0 \end{cases}, \quad (17)$$

where b is a characteristic swimmer dimension. While the evolution of the swimmer position \mathbf{x}_2 , is clear from the relation 17, we still need to ascertain the evolution of the swimmer orientation \mathbf{p} , when it is close to the surface. The swimmer orientation is affected deterministically by Ω_{HI} , and randomly via the Gaussian white-noise (rotary diffusion, D_r) and the Poisson process (tumbling, equation 10). It is the third behavior that we need to treat carefully, keeping in mind how surfaces affect bacterial tumbling. As stated by Elgeti *et al.* in a recent review article, “The swimming behavior of bacteria close to surfaces differs from the run-and-tumble motion in free solu-

tion” [53]. This difference in swimming behavior is well-documented in prior experimental studies [12–15, 22, 72]. Specifically, it is known that tumbling of the bacterium *E. coli* is reduced by as much as $\approx 50\%$ in the proximity of solid surfaces [22, 72]; and that *E. coli* can escape these surfaces not by tumbling away, but by diffusing their orientation away from the surface and then swimming away [20, 21]. Even in the event that a tumble does occur, the post-tumble orientations are mostly restricted to the tangent plane at the location of the bacterium. The near interface behavior of marine bacteria—that do not necessarily utilize the run-and-tumble motion of *E. coli*—has

not been investigated in detail. Therefore, we take an empirical approach to near surface tumbling and postulate that the microorganism ceases to tumble at distances from the solid surface that are less than twice the swimmer's body-length. The rotary diffusion of a bacterium on the other hand, is independent of its ability to tumble, or display other motility traits [3]. It is a well known behavior of most bacterial species, both enteric and marine, and is attributed to thermal fluctuations and/or intrinsic irregularities. Therefore, the ' D_r term' influences the orientation \mathbf{p} of the microorganism irrespective of its distance from the surface. In summary, the microswimmer motion in the bulk (> 2 body-lengths separation) is governed by equations 6, 8, 10, 15 and 16; while that near the surface (< 2 body-lengths separation) is governed by 8 and 17. In what follows, we numerically solve these equations for sufficiently large number of instances, to get statistically meaningful results and deduce the effect of the various mechanisms (see Table I) on the distribution

of microswimmers around spherical nutrient sources.

III. RESULTS & DISCUSSION

A. Interplay between hydrodynamic interaction and chemotaxis

We select the following scales to non-dimensionalize the various quantities of interest: lengths by the characteristic swimmer dimension b ($1 \mu\text{m}$), speeds by the swimming speed V_s ($10 \mu\text{m/s}$), time by b/V_s (0.1 s), dipole strength by $\mu b^2 V_s$ ($0.01 \text{ pN}\cdot\mu\text{m}$), nutrient concentration by K_D , and rotary diffusivity by V_s/b (10 s^{-1}). This yields the important dimensionless parameters, along with their orders of magnitude, in our study to be: radius of the source $A = R/b \approx 20 - 60$, dipole strength $\alpha_D = F/(8\pi\mu b^2 V_s) \approx 0.1 - 2.0$ ($F \approx 0.1 - 10 \text{ pN}\cdot\mu\text{m}$), diffusivity $D = D_r b/V_s \approx 10^{-5} - 10^{-3}$, surface concentration (representative nutrient availability) $C_0/K_D \approx 10^{-2} - 10^2$, and run-time (or equivalently, inverse of tumbling frequency) $\tau^* = \tau_0 V_s/b \approx 4 - 12$.

TABLE I. Summary of various mechanisms dictating swimmer behavior near a rigid, spherical surface exuding a chemoattractant with a specified concentration at the surface of the source.

Mechanism: dimensionless parameter	Contribution
Hydrodynamic interaction (H.I.): α_D and A	attraction of nearby swimmers leading to scattering/trapping
Chemotaxis: C_0/K_D and τ^*	initial attraction of distant swimmers towards the nutrient source
Hardcode repulsion: $ \mathbf{x} /b \leq 1$	balance with H.I. leads to orbiting/entrapment
Rotary diffusion: D	orientational fluctuations may cause the swimmer to escape from surface

In our simulations, the baseline parameters are: $\alpha_C = 300 \text{ s}$, $C_0/K_D = 1.0$, $\tau^* = 6$, $\alpha_D = 0.8$ or 10^{-3} , $A = 20$, $D = 7.5 \times 10^{-4}$ (or, $D \approx 0$, when rotary diffusion is neglected). The swimmer dynamics is solved for 10000 instances, each running up to 200 dimensionless time units ($t_{end} = 200$). In each case, the initial position of the swimmer is 20 body-lengths away from the source ($|\mathbf{x}_2(0)| = 40$), and the initial orientation is randomly assigned. The final result that we investigate is the distribution of the swimmers' locations $r(= |\mathbf{x}_2|)$ at the end of the simulations. We compute two different quantities of interest: (i) a 'surface concentration' C_s , and, (ii) a radial distribution function $f(r)$. C_s is the fraction of the total microorganisms that get trapped at the surface, i.e., those whose trajectory end-point lies within a separation of 1.5 body-lengths from the source. It is a measure of the surface colonization by the bacteria. $f(r)$ is a distribution function such that the fraction of microorganisms

that lie in a thin spherical shell of radius dr is equal to $4\pi r^2 f(r) dr$. In other words, the probability of finding a microorganism between r and $r + dr$ is proportional to $4\pi r^2 f(r) dr$. $f(r)$ is normalized such that together with C_s , it satisfies

$$C_s + \int_{r=A}^{\infty} 4\pi r^2 f(r) dr = 1. \quad (18)$$

A confluence of chemotaxis, hydrodynamics, 'hardcore repulsion' and rotational diffusion shapes the behavior, and subsequent distribution of the swimming microorganisms around the source. Before proceeding to isolate the effects of each of these, we provide a qualitative description of the important physico-chemical interactions taking place. Spagnolie *et al.* used solely hydrodynamics based arguments to show that if the radius of a spherical obstacle is larger than a 'critical trapping radius', then

it can hydrodynamically capture/trap swimmers that directly impinge upon it (see Fig. 2(a)). Alternatively, swimmers with dipole strengths larger than a critical value can get hydrodynamically trapped around spherical obstacles (see Fig. 2(b)). In addition, for all cases where hydrodynamic trapping is expected to occur, there exists a ‘basin of attraction’ such that tangentially directed pusher swimmers that lie within the basin get trapped and travel along the surface of the sphere (see Fig. 2(c)). The ‘depth’ of this basin varies with the sphere radius A , and the dipole strength α_D . It is at most 2.5 body-lengths for A as large as 200 and $\alpha_D = 0.8$. At such small separations, Molaei *et al.* have shown the inability of an *E. coli* cell to tumble, or even escape the solid surface [22, 72]. Therefore, hydrodynamics is strongest, and tumbling weakest, when the microorganism is located very close to the source. Conversely, when the microorganism is far from the source, the hydrodynamics becomes negligible and chemotaxis is the dominant factor in dictating its motion.

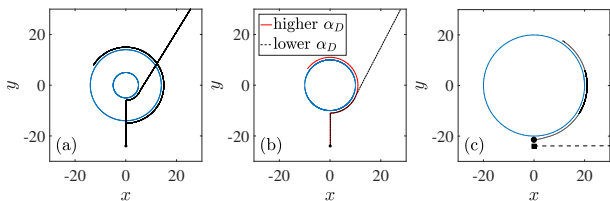


FIG. 2. (a) The concept of the critical trapping radius [25]: the swimmer trajectory around the smaller sphere escapes, while that around the larger sphere (whose radius is greater than a critical trapping radius) gets trapped. The swimmers’ initial orientation, $\mathbf{p}(0) = \mathbf{e}_Y$. (b) Alternatively, for a fixed radius, only the swimmer with α_D larger than a ‘critical dipole strength’ will get trapped around the sphere. (c) The concept of the basin of attraction [25]: the swimmer whose initial location is marked by a circle (resp. square) and whose trajectory is shown by a solid line (resp. by a dashed line), starts inside (resp. outside) the basin of hydrodynamic attraction, and thus it gets trapped onto (resp. escapes) the surface. The swimmers’ initial orientation, $\mathbf{p}(0) = \mathbf{e}_X$. It is important to note that the basin of attraction is defined only in cases when hydrodynamic trapping is ensured.

Thus, a bacterium located far away from the source can get attracted to, and even trapped onto, it via the following sequence of events: (i) chemotaxis, i.e., biased tumbling causing the bacterium to come within 2-3 body lengths from the source, followed by (ii) hydrodynamic attraction on account of the theory detailed in Sections II A and II C. Once the bacterium reaches the nutrient, its behavior is governed by the interplay of: (i) hydrodynamics, (ii) hard-core repulsion, and (iii) rotary diffusion. The interaction between the first two may result in the trapping of the microorganism, depending on its dipole strength and the radius of the source. If the radius is larger than the critical trapping radius (corresponding to the swimmer’s dipole strength), then the bacterium will

be trapped at the surface—due to a balance between hydrodynamic attraction and hardcore repulsion—and will orbit around the source. The third effect contributes toward probable escape of any bacterium that would get trapped onto the surface based purely on hydrodynamics. The escape can occur due to a reorientation that turns the bacterium to an extent that $(\mathbf{u}_{HI} + V_s \mathbf{p}) \cdot \hat{\mathbf{r}} > 0$ (see equation 17), thus allowing it to swim away from the surface. This three-way coupling has been explained schematically in Fig. 3, and discussed in greater detail in ref. [25, 26]. Note also that rotary diffusion causing swimmer escape (for a variety of microorganisms) from solid surfaces has also been observed experimentally in ref. [20, 21, 42].

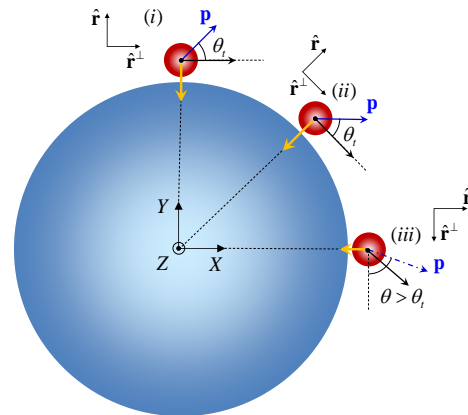


FIG. 3. (Color online) An illustration of the effect of hydrodynamics on the motion of the microorganism as it gets trapped onto the surface of the nutrient source. The thin blue arrows are the swimmer’s intrinsic motility $V_s \mathbf{p}$, the thick orange arrows are the hydrodynamic component of swimmer’s motion toward the center of the nutrient $(\mathbf{u}_{HI} \cdot \hat{\mathbf{r}})$, and the black arrows are the instantaneous velocity of the swimmer, $d\mathbf{x}_2/dt$ (eqn. 17). (i-ii) Hydrodynamics—if strong enough—rotates the swimmer such that it always maintains a constant separation $h_t (\approx 1)$ and in-plane angle θ_t , and such that $(\mathbf{u}_{HI} + V_s \mathbf{p}) \cdot \hat{\mathbf{r}} \leq 0$. As a result, the swimmer swims tangentially along the surface and stays trapped. (iii) Rotary diffusion—if significant—can cause the swimmer to rotate to an in-plane angle greater than θ_t which reduces the hydrodynamic attraction, causes $(\mathbf{u}_{HI} + V_s \mathbf{p}) \cdot \hat{\mathbf{r}} > 0$, and thus leads to swimmer escape.

Quantitatively, it suffices to remember that hydrodynamic trapping is most favored for high values of α_D and low values of D . This is because large α_D results in stronger hydrodynamic attraction, and small D reduces the influence of rotary diffusion. We further explain this idea in the next Section. Table I summarizes the influence of the mechanisms discussed above, on the fate of a microorganism located initially at some arbitrary distance from the source, and oriented along any arbitrary direction. Fig. 4 shows typical trajectories and provides an understanding of microorganism distribution around the source for the case of strong and weak chemotaxis; in

the subsequent sections we quantify these results.

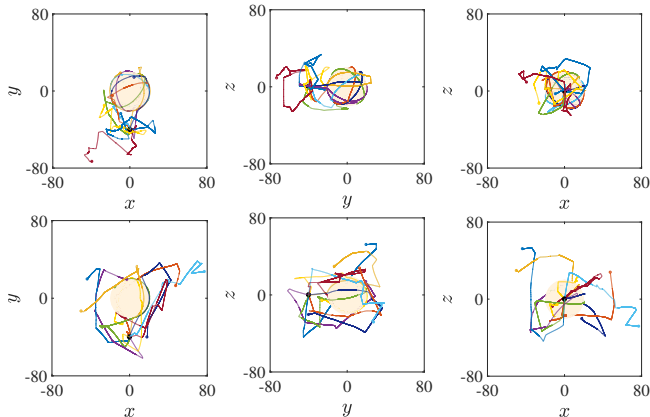


FIG. 4. (Color online) A schematic of the effect of chemotaxis strength on the accumulation around the nutrient source. The left, central and right columns show the x - y , y - z and x - z projections, respectively, of the microorganisms' trajectories. The swimmers are located initially at $(x(0), y(0), z(0)) = (0, -40, 0)$, and oriented arbitrarily. It is important to note that in the absence of chemotaxis, most of the swimmers would just 'swim away' from the source without appreciably changing their orientations. The upper (resp. lower) row represents strong (resp. weak) chemotaxis, which could either be due to $C_0/K_D = 1.0$ (resp. $C_0/K_D \ll 1.0$), or a small (resp. large) value of τ^* . Clearly, strong (resp. weak) chemotaxis leads to the swimmers being, in general, closer to (resp. further from) the nutrient.

B. Types of behaviors

Fig. 5 provides us with an intuition about the different physical mechanisms dictating microorganism attraction and entrapment onto nutrient sources. It contains features of run-and-tumble chemotaxis as well as hydrodynamic trapping. We see that chemotaxis doesn't always succeed in bringing the microorganism to the source (red trajectory); or that chemotaxis can lead the microorganism close enough to the source but still outside its basin of attraction (blue trajectory). In the case shown by the magenta trajectory, we see how chemotaxis allows a microorganism to make 'contact' with the source but it later gets scattered instead of being trapped. Finally, we also see how chemotaxis and hydrodynamics enable the microorganism to make 'contact' with the source and then glide along its surface due to hydrodynamic entrapment (green trajectory). This rich variety of trajectories emerges due to an interplay involving varying strengths of one or all of the mechanisms detailed in Table I. It is clear that the phenomena being investigated is very non-trivial in all its complexity. A better understanding can be obtained by first considering limiting values of certain parameters, and then moving on to more general parametric regimes. In particular, an understanding of the

limiting scenarios $D \approx 0$ and/or $\alpha_D \approx 0$ is warranted. We will see that both these parameters play an important role in the extent of surface colonization C_s , and the nature of the distribution function $f(r)$.

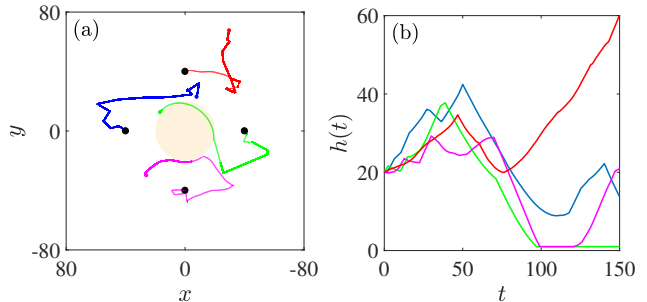


FIG. 5. (Color online) (a) Visualization of the different behaviors elicited by the mechanisms discussed in Table I. The starting positions are shown by black dots. Red: this microorganism is unable to locate the source in the time for which the simulations were run. Blue: this microorganism 'chemotaxes' close enough to the source, but does not enter the basin of hydrodynamic attraction. Magenta: in this case, the microorganism does make contact with the source, but the hydrodynamic attraction is not strong enough for trapping to occur. Green: an example of a successful trapping wherein chemotaxis and hydrodynamics work in conjunction to bring and trap a microorganism onto the source. See main text for details about the regimes in which such behaviors occur. (b) The time evolution of the distance from the source, $h(t)$, of trajectories in panel (a).

C. Influence of the dipole strength α_D and the rotary diffusivity D

Fig. 6(a) shows the variation in C_s with α_D for $D \approx 0$ and $D = 7.5 \times 10^{-4}$. The corresponding bulk distributions $f(r)$ are shown in Fig. 6(b). The other parameters are kept at their baseline values, such that chemotactic approach is guaranteed in most cases. The bulk concentration is highest near the surface and reduces monotonically to zero as r increases. This shows that chemotaxis, on average, helps the microorganisms to locate nutrient rich regions in their surroundings.

We note that for $D \approx 0$, the response is binary, i.e., C_s is either ≈ 0.155 or ≈ 0.60 and $f(r)$ varies as one of the two discernible curves in the main plot of Fig. 6(b). This is because in the absence of orientational fluctuations, swimmers that enter the basin of attraction (through chemotaxis) behave deterministically: they either get trapped or they escape. For a given size of the source ($A = 20$ in all our results), the type of behavior—both qualitative *and* quantitative—depends only on the value of α_D : (i) for large enough α_D , a majority of swimmers get trapped at $r \approx 20$; while, (ii) for smaller α_D , a majority is collected at the bulk (recall Fig. 2(b)). This behavior can be understood by considering the dependence

of hydrodynamic interactions on the dipole strength and on the distance of the microorganism from the source. At large distances, hydrodynamics has a negligible impact on reorienting the bacteria, and they behave more or less similarly, irrespective of their α_D values. However, once inside the basin, the fate of a bacterium (trap or escape) depends acutely on α_D ; and for a given size A , any bacterium with α_D above (resp. below) a critical value gets hydrodynamically trapped (resp. escapes). In fact, for a fixed A , purely hydrodynamics based trapping occurs above a critical $\alpha_D \geq 8/(3A^{1/2})$ [25]. Therefore, for $A = 20$, trapping should occur for $\alpha_D \geq 0.65$, as evident in Fig. 6. Even then, the randomness of the initial approach means that $C_s < 1$, i.e., not all swimmers get trapped (recall the red and the blue trajectories in Fig. 5).

Another feature of the results in this Section is that higher C_s values imply a lower average value of $f(r)$. This allows us to identify the regions where most of the microorganisms accumulate. In all scenarios when $C_s < 0.2$, the nature of $f(r)$ is such that $\int_A^{2A} 4\pi r^2 f(r) dr \approx 0.5$. This can be interpreted as an ‘off-surface’ accumulation. It occurs due to an efficient chemotactic approach combined with weak hydrodynamic attraction; causing most swimmers to gather within one (source) radius from the surface.

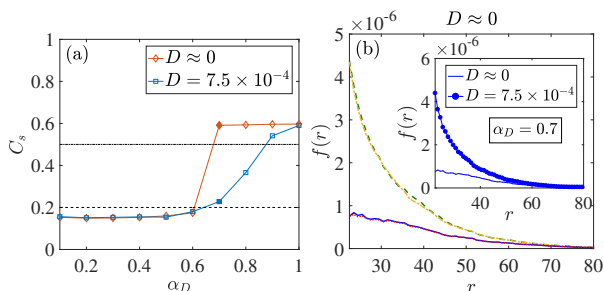


FIG. 6. (Color online) (a) Variation of the surface concentration, C_s , with the dipole strength α_D for $D \approx 0$ (negligible rotary diffusion), and $D = 7.5 \times 10^{-4}$ (moderate rotary diffusion). (b) Main figure: The distribution $f(r)$ as a function of α_D for $D \approx 0$, and $\alpha_D = 0.1$ (green dashed line), $\alpha_D = 0.6$ (orange dash-dotted line), $\alpha_D = 0.7$ (blue solid line), $\alpha_D = 1.0$ (red dotted line). Inset: The distribution $f(r)$ for $\alpha_D = 0.7$ for $D \approx 0$ and 7.5×10^{-4} (corresponding surface concentrations are shown in panel (a) by filled symbols). Notice the drastic difference in the values of C_s and $f(r)$ for the two different of rotary diffusivities.

As a swimmer with $\alpha_D \geq 0.65$ comes in contact with the source, it begins to travel along the surface due to the mechanisms explained in Fig. 3. The only mechanism that can get such a trapped swimmer to escape is its own rotary diffusivity. This idea was explained schematically in Fig. 3 and an example of such an escape can be seen in the magenta trajectory of Fig. 5. Fig. 6(a) shows (blue line marked with squares) the variation of C_s with α_D for $D = 7.5 \times 10^{-4}$. It can be seen that rotary diffusiv-

ity markedly affects the tendency of the microorganism to accumulate at the surface and consequently, results in more swimmers in the fluid surrounding the source (inset in Fig. 6(b)). For example, for $\alpha_D = 0.7$ there is $\approx 60\%$ reduction (resp. increment) in surface colonization (resp. average bulk distribution) for a modest rotary diffusivity. As the strength of hydrodynamic attraction grows (α_D increases) a greater fraction of the swimmers get trapped at the surface, in spite of orientational fluctuations. Therefore, the near-field hydrodynamic attraction acts as a crucial mechanism that allows microorganisms to colonize nutrient sources.

Finally, whenever hydrodynamic attraction is weak ($\alpha_D < 0.65$), the rotary diffusivity does not affect the surface concentration at all (values of C_s for $D \approx 0$ and $D > 0$ are coincident for $\alpha_D < 0.65$, for a wide range of D). This is understandable because if hydrodynamic interactions are weak, the swimmer just doesn’t rotate fast enough to stay trapped onto the surface, and thus its escape is guaranteed regardless of other influences (see Fig. 3). The very weak dependence on D comes from the fact that far away from the source—where the swimmers predominantly reside—orientational changes due to rotary diffusivity are negligible as compared to those due to a tumble; as also seen for collective motion of active suspensions [73]. Fig. 10 in the Appendix shows that the bulk distributions are also practically identical in this case.

D. Variability in chemotactic factors: C_0/K_D and τ^*

In Section III C, we saw the importance of hydrodynamics in trapping chemotactic microorganisms onto the source. We also explained how rotary diffusivity of the swimmers reduces surface colonization. The main question that we aim to answer in this Section is: how does chemotaxis-based initial approach affect the colonization of nutrient sources by bacteria? There are two factors that we need to consider: (i) nutrient availability in the form of a prescribed background concentration, and, (ii) the microorganism’s intrinsic response to gradients in nutrient concentration. The nutrient availability—which is an environmental factor—is quantified by the ratio C_0/K_D . Thus, it could be an indication of the actual concentration of a given chemoattractant at the source (e.g., the amount of soluble hydrocarbons in a drop of crude oil), or the affinity of the chemoreceptor to the chemoattractant [32]. The intrinsic chemotactic response—which is a motility trait of individual bacteria—depends on the mean tumbling frequency τ_0^{-1} .

Does greater nutrient availability enhance the colonization of nutrient sources by bacteria? Fig. 7(a) shows that this is not necessarily the case, irrespective of the hydrodynamic influences. The C_s vs. C_0/K_D trend for all combinations (high/low) of α_D and D is the same: an approximately two-fold initial increase, followed by no change for a wide range of C_0/K_D , and then a re-

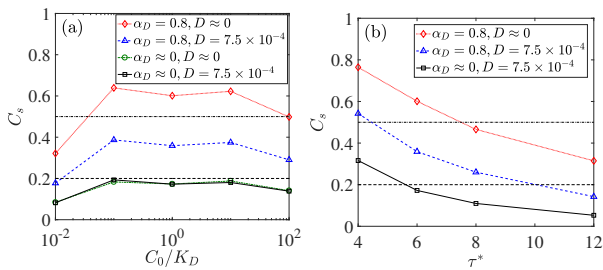


FIG. 7. (Color online) Variation of the surface concentration C_s with (a) C_0/K_D , and, (b) τ^* . In each case, C_s is highest when $\alpha_D > 0.65$ and D is negligible, as expected based on the discussion in Section III C. Also, the results are independent of D for $\alpha_D \approx 0$. For small τ^* , C_s varies almost linearly with τ^* .

duction. There isn't much difference in the surface concentration (and the bulk distribution; see Fig. 8(a)) between $C_0/K_D = 0.1, 1.0, 10.0$. This behavior is explained by the scaling of the run-time τ with C_0/K_D , which can be easily assessed by examining equation 16. If $C_0 \ll K_D$, then $\tau/\tau_0 \sim \exp(DC/Dt)$; if $C_0 \sim K_D$, then $\tau/\tau_0 \sim \exp(C^{-1}DC/Dt)$; and if $C_0 \gg K_D$, then $\tau/\tau_0 \sim \exp(C^{-2}DC/Dt)$ [2]. This means that higher nutrient availability doesn't always result in a proportionate increase in the run-time τ in nutrient-rich regions, and so, it doesn't necessarily translate to improved chemotactic performance. In fact, if C_0/K_D is increased even further to 100.0, then we observe a decline in C_s as compared to the previous three cases, due to the dominant contribution of the C^{-2} term, as described above. Physically, $C_0 \ll K_D$ would mean that the ambient nutrient concentration is not high enough to prompt rapid chemotaxis, while the other extreme $C_0 \gg K_D$ is equivalent to a nutrient abundance that makes 'chemotactic foraging' unnecessary.

The chemotactic response of bacteria is much more sensitive to τ^* (dimensionless run time), than it is to C_0/K_D . The variation of C_s with respect to τ^* is monotonic, and bacteria with lower mean run-lengths are much more effective in colonizing nutrient sources. Fig. 7(b) shows that surface colonization can be as high as 80 % for $\tau^* = 4$. The green trajectory of Fig. 5 is a good example of such strong surface colonization, wherein chemotaxis enables the microorganism to make contact with the source and strong hydrodynamic attraction keeps it trapped at the surface. Owing to their random initial orientations, it is essential for the distant bacteria to tumble more frequently in order to 'locate' the source. This is why bacteria with smaller τ^* values are able to orient themselves along ∇C —and ultimately enter the basin of hydrodynamic attraction—faster than those with larger τ^* , and high C_s values for the former are just a consequence of this rapid chemotactic response.

An inspection of Fig. 8 in the context of Fig. 7 enables us to draw useful conclusions about the bacterial distribution in the bulk for different values of C_0/K_D and τ^* .

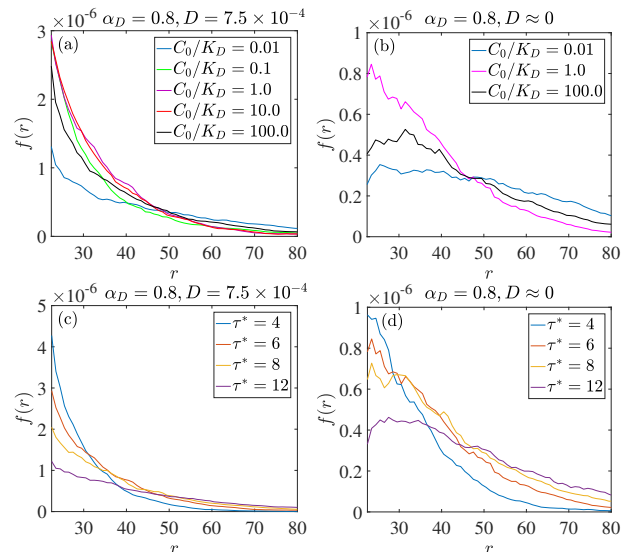


FIG. 8. (Color online) The bulk distribution $f(r)$ as a function of (a-b) C_0/K_D , and, (c-d) τ^* . Note the almost similar distributions for $C_0/K_D = 0.1, 1.0, 10.0$, just like the corresponding C_s values in Fig. 7. In conjunction with Fig. 7, it is evident how rotary diffusion causes more microorganisms to stay in the bulk. For weak chemotaxis, there is no appreciable accumulation anywhere in the bulk. $f(r)$ increases to a maximum and then decays to zero for weak chemotaxis in the panels (b) and (d). See main text for details.

A general observation from Fig. 7 is that chemotaxis can be considered 'strong' (resp. 'weak') whenever $C_0/K_D \approx O(1)$ (resp. $C_0/K_D \ll 1$) and/or $\tau^* < 8$ (resp. $\tau^* > 8$). We see that the value of $f(r = 20)$ and the subsequent decline of $f(r)$ is much more gradual for weak chemotaxis (Fig. 8(a) and (c)), with $\int_A^{4A} 4\pi r^2 f(r) dr \approx 0.5$. This suggests insignificant accumulation at any particular location because the chemotactic bias isn't strong enough. The curves for $C_0/K_D = 0.01, 100$ in Fig. 8(b), and for $\tau^* = 12$ in Fig. 8(d) exemplify the scenarios when hydrodynamic attraction is strong enough to promote surface-aggregation, but the initial approach toward the source is highly hindered. As opposed to all other cases, these distributions exhibit a gentle maximum at a distance $r \approx 30$. This is an interesting aspect of the present study: the existence of a 'depletion zone' in the bulk distribution of swimmer positions for all scenarios involving strong hydrodynamics and weak chemotaxis. In spite of the latter effect, some swimmers do encounter the source and get trapped onto it; while others move in an almost random fashion. The depletion zone spatially demarcates these two extremes.

IV. CONCLUSION

We formulated a mathematical model and performed probabilistic simulations to ascertain the distribution of

microorganisms around a spherical nutrient source. The model was based on, and the distribution was mediated by, a combination of (i) hydrodynamic interaction (H.I.) with the source, and, (ii) chemotaxis toward the nutrient/chemoeffector emanating from the source. In our model, we assumed that hydrodynamic interactions and rotary diffusion dominate in the near-field of the nutrient source, while chemotaxis dominates when the microorganism is far away. This distinction stems from the fact that bacterial tumbling is hindered in the proximity of solid surfaces (thus precluding run-and-tumble chemotaxis and surface-escape via tumbling) [22], and so near surface bacterial behavior is governed by hydrodynamics in conjunction with rotary diffusion [20, 21, 25]. Hydrodynamic interactions can be strong or weak, depending on the value of the microorganism’s dipole strength and the radius of the source. Chemotaxis too, can be strong or weak, depending on the microorganism’s mean tumbling frequency, and the nutrient availability in its surroundings. Therefore, the distribution is affected by environmental (source size and nutrient availability) factors, as well as by the microorganism’s intrinsic motility features (dipole strength, tumbling frequency, etc.). Although both hydrodynamics and chemotaxis attract a bacterium toward the source, their separate ‘domains of influence’ and relative strengths can lead to interesting changes in the spatial distribution of microorganisms around the surface from which the nutrient diffuses out into the environment. Towards this, we performed a systematic parametric study and revealed different surface colonization and bulk distribution features, highlighted in Fig. 9.

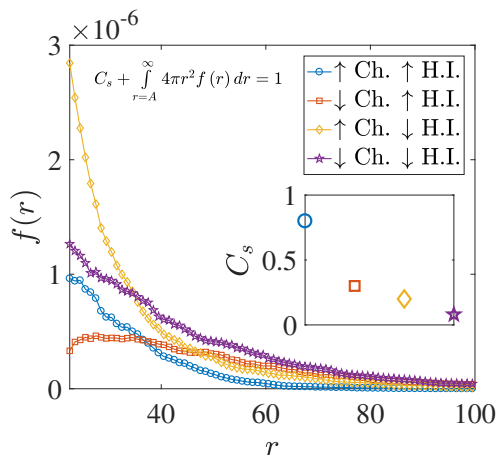


FIG. 9. (Color online) The four qualitatively different behaviors, or spatial distributions $f(r)$, that can be realized due to the combined influence of hydrodynamics (abbreviated in the legend as H.I.) and chemotaxis (abbreviated in the legend as Ch.) on the locomotion of microorganisms around a spherical nutrient source. \uparrow (\downarrow) denotes a strong (weak) influence. The inset shows the surface colonization C_s for each of the four behaviors, with correspondence based on marker type.

We see that stronger H.I. always leads to greater sur-

face colonization (i.e., the quantity C_s), irrespective of the strength of the chemotactic influence. Similarly, stronger chemotaxis always leads to greater surface colonization, irrespective of the strength of the hydrodynamic influence. Understandably, C_s is greatest when both the influences are strong, because this scenario corresponds to a more effective ‘initial approach’ (toward the source) due to chemotaxis, followed by a strong hydrodynamic attraction. On the other hand, it is the least when both chemotaxis and H.I. are weak. The surface colonization is also not substantial ($C_s < 0.5$) whenever chemotaxis or H.I. is weak. Strong chemotaxis, but weak H.I. leads to an off-surface accumulation with majority of microorganisms collecting in the bulk within a distance of one (source) radius from the surface. Finally, we find an interesting bulk distribution for the case of weak chemotaxis and strong H.I., which leads to the formation of a depletion zone in the swimmer distribution, characterized by a gentle maximum in the value of $f(r)$ at $r \approx 30$. This is because weak chemotaxis does not enable enough swimmers to come close to the source, but those that do come close enough, get trapped due to strong hydrodynamic attraction. These sufficiently general trends help establish the importance of chemotaxis and hydrodynamics in our problem. From them, we conclude that strong chemotaxis is essential to obtain greater aggregation of microorganisms near nutrient sources, and strong hydrodynamic interactions enable surface colonization. In addition to these generalities, we also find that higher nutrient availability—reflected in the value of the dimensionless parameter C_0/K_D —doesn’t lead to proportionate increase in surface colonization (see Fig. 7(a)). This is because the bacterium’s run-length τ depends on both its ambient nutrient concentration, C , and the instantaneous rate at which this concentration changes, DC/Dt , via eqn. 16. However, strong chemotaxis on account of lesser mean run time τ_0 is much more effective in enhancing the surface colonization (see Fig. 7(b)). In this way, our study yields a qualitative and quantitative insight into the process of bacterial attraction to, and aggregation around, nutrient sources under the combined influence of the two major factors dictating microorganism locomotion: passive response via hydrodynamics and active response via chemotaxis.

An important assumption in our study is that tumbling, and hence chemotaxis, is suppressed when the swimmer is at a distance less than or equal to two body-lengths from the source. The basis of this assumption is the experimental work by Molaei *et al.* which confirmed tumbling suppression near rigid walls [22, 72]. In addition, we use the model proposed by Brown and Berg to incorporate bacterial chemotaxis [2], and neglect any ‘memory effects’ when calculating the run time in presence of a chemoeffector (see equation 16). We emphasize that the finer aspects of chemotaxis can be easily incorporated into our study, like tumbling anisotropy enforced due to proximity to surfaces and/or due to altogether different foraging tactics like reversals and flicks.

It would be interesting to see the extent to which these influences affect the results of our study. Equally interesting is the possibility of studying hydrodynamic interactions between microswimmers in the dilute or semi-dilute regime, and how it would affect their spatial distribution around nutrient sources. A more complex mathematical model—one which includes some, or all, of the aforementioned effects—would require experiments to ascertain tumbling alteration close to curved surfaces, and predict bacterial re-orientations differing from the archetypal tumble. The present study improves our understanding of bacterial colonization of surfaces, and is expected to have far reaching consequences in bioremediation, selective microorganism capture, lab-on-a-chip assays and investigations on bacteria in porous media.

APPENDIX

In Fig. 7 we saw that rotary diffusivity has no effect on the surface colonization when hydrodynamic effects are negligible, i.e., $\alpha_D \approx 0$. Fig. 10 shows that even the bulk distribution is not affected significantly in this case. This is because for $\alpha_D \approx 0$, the microorganisms execute a biased random walk and get reflected from the surface irrespective of the magnitude of rotary diffusion, as explained in Section III C.

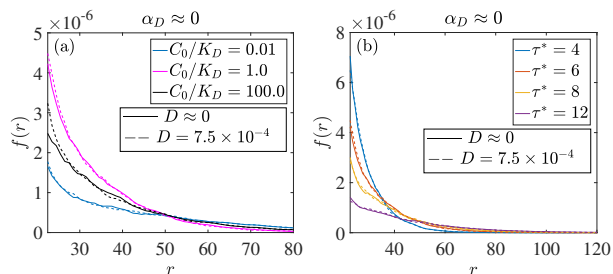


FIG. 10. (Color online) The bulk distribution $f(r)$ as a function of (a) C_0/K_D , and, (b) τ^* , for negligibly small hydrodynamic attraction ($\alpha_D \approx 0$) and $D \approx 0$, $D = 7.5 \times 10^{-4}$.

In Section II B we mentioned that the effect of rotary diffusion as given by eqn. 8 is strictly correct only if the rotary diffusion tensor—say \mathbf{D}_R —is isotropic, i.e., when $\mathbf{D}_R = D_r \mathbf{I}$. In reality, the presence of a surface and the approach of bacterium to the spherical source imparts anisotropy and time dependence, respectively, to \mathbf{D}_R . The stochastic effects become considerably involved when the diffusivities evolve with time (see eqns. (13) and (14) in ref. [56]). However, in our problem, fluctuations in the bacterial orientation are only important in the near-field, i.e., when a bacterium orbits around the source (see Fig. 5, Table I and the discussion in the last paragraph of Section III C in relation to Fig. 6(a) and Fig. 10). Also, the change in $\|\mathbf{D}_R\|$ for a sphere is most significant when it is very close to touching a solid wall [74–76]. In fact, using the mobility expressions given

by Cichocki and Jones [75] we can estimate that $\|\mathbf{D}_R\|$ is halved when a sphere almost makes contact with the wall (assuming, of course, that their results can be reasonably used for our configuration of two spheres—the source and the bacterium—because $R/b \gg 1$). Therefore, the D_r in eqn. 8 can be considered as the ‘reduced’ rotary diffusivity due to close proximity to a surface. In other words, if the rotary diffusivity in the unbounded fluid is D_{r0} , then that near the source will be $D_r = kD_{r0}$, where $k \approx 1/2$. Note that using two different values of D_r :

$$D_r = \begin{cases} D_{r0}, & |\mathbf{x}_2| \gg (R+b) \\ \frac{D_{r0}}{2}, & |\mathbf{x}_2| \approx (R+b) \end{cases}, \quad (19)$$

instead of using only $D_r = (D_{r0}/2)$ everywhere in the domain, will not change our results appreciably, once again because of the near-field significance of rotary diffusion (see Fig. 11).

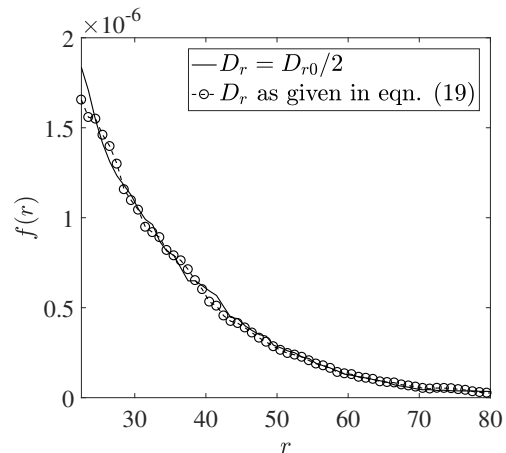


FIG. 11. (Color online) The bulk distribution $f(r)$ for two different cases: (i) when the value of D_r in eqn. 8 is taken to be half of the quiescent rotary diffusivity D_{r0} in the *entire* domain (solid line), and, (ii) when eqn. 19 is used to assign bacterial rotary diffusivities based on separation of the microorganism from the source (dashed line marked with circles). The surface colonization values are within 1.25% of each other. The value of the dimensionless rotary diffusivity in unbounded fluid is 7.5×10^{-4} , i.e., $D_{r0}b/V_s = 7.5 \times 10^{-4}$.

The methodology outlined in Section II also enables us to compute the distribution of microorganisms around more general surfaces, for example, that near fluid-fluid interfaces. The fundamental difference in this case is that the boundary conditions change from those given in eqn. 3, to the more general form of continuity of fluid velocity and stress [43]. As a result, for microorganism motion around clean drops, the viscosity ratio of the drop with respect to the suspending fluid—denoted by λ —appears as an extra parameter that can dictate the distribution function $f(r)$. This change is reflected in the expressions for \mathbf{u}_{HI} and $\mathbf{\Omega}_{HI}$, which were derived recently by Shaik and Ardekani [48]. If we assume that the near field hydrodynamic and tumbling characteristics remain

the same as those in Section II C, and that the microorganism does not simply adsorb onto the drop's surface, we can estimate the distribution of chemotactic bacteria around drops as well. Fig. 12 shows the spatial distribution of chemotactic microorganisms around a stationary drop with viscosity ratio 10, which is indicative of crude oil [77]. The distribution is almost the same as that around a rigid, spherical nutrient source (limiting case of $\lambda \rightarrow \infty$); thus suggesting the utility of our results in the analysis of biodegradation of hydrocarbon effusing crude oil drops.

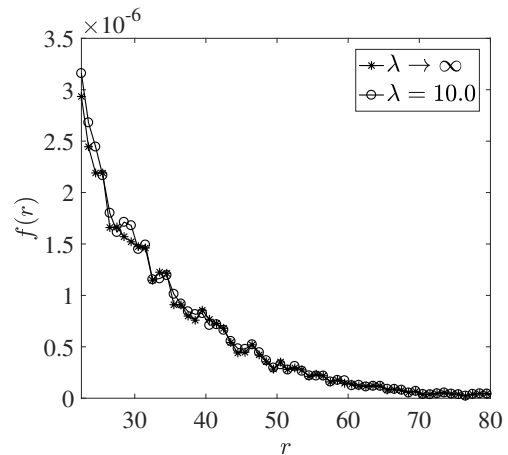


FIG. 12. Comparison of the bulk distribution $f(r)$ for combined chemotactic and hydrodynamic attraction to (i) a rigid sphere (asterisks), and, (ii) a clean drop with viscosity ratio $\lambda = 10$ corresponding to crude oil (circles), for the baseline simulation parameters given in Section III A. The difference between the two cases is not very significant. The surface colonization for the rigid sphere ($C_{s,\text{rigid}} = 0.3589$) is 4 % larger than that for the drop ($C_{s,\text{drop}} = 0.3446$). For motion around the drop, the hydrodynamics induced linear and angular velocities are taken from ref. [48].

ACKNOWLEDGEMENTS

This research was made possible by grants from the Gulf of Mexico Research Initiative and the NSF, CBET-1445955-CAREER and CBET1604423. The authors thank Dr. Roseanne M. Ford for useful discussions. ND would like to thank Dr. Aditya Bandyopadhyay for useful discussions. The authors also thank the anonymous referees for their suggestions in improving the quality of this manuscript. Data are publicly available through the Gulf of Mexico Research Initiative Information & Data Cooperative (GRI-IDC) at <https://data.gulfresearchinitiative.org> (DOI: 10.7266/N7GQ6W92).

-
- [1] H. C. Berg and D. A. Brown, *Nature* **239**, 500 (1972).
 - [2] D. A. Brown and H. C. Berg, *Proceedings of the National Academy of Sciences* **71**, 1388 (1974).
 - [3] H. C. Berg, *Random Walks in Biology.*, 2nd ed. (Princeton, Princeton, New Jersey, 1993).
 - [4] H. C. Berg, *E. coli in Motion* (Springer-Verlag, New York, NY, 2004).
 - [5] M. Eisenbach, J. Lengeler, M. Varon, D. Gutnick, R. Meili, R. Firtel, J. Segall, G. Omann, A. Tamada, and F. Murakami, *Chemotaxis* (Imperial College Press, London, 2004).
 - [6] H. Szurmant and G. W. Ordal, *Microbiology and Molecular Biology Reviews* **68**, 301 (2004).
 - [7] G. H. Wadhams and J. P. Armitage, *Nature Reviews Molecular Cell Biology* **5**, 1024 (2004).
 - [8] R. Lux and W. Shi, *Critical Reviews in Oral Biology & Medicine* **15**, 207 (2004).
 - [9] S. L. Porter, G. H. Wadhams, and J. P. Armitage, *Nature Reviews Microbiology* **9**, 153 (2011).
 - [10] R. Stocker, *Proceedings of the National Academy of Sciences* **108**, 2635 (2011).
 - [11] E. Lauga and T. R. Powers, *Reports on Progress in Physics* **72**, 096601 (2009).
 - [12] W. R. DiLuzio, L. Turner, M. Mayer, P. Garstecki, D. B. Weibel, H. C. Berg, and G. M. Whitesides, *Nature* **435**, 1271 (2005).

- [13] E. Lauga, W. R. DiLuzio, G. M. Whitesides, and H. A. Stone, *Biophysical Journal* **90**, 400 (2006).
- [14] L. Lemelle, J.-F. Paliere, E. Chatre, and C. Place, *Journal of Bacteriology* **192**, 6307 (2010).
- [15] R. Di Leonardo, D. Dell’Arciprete, L. Angelani, and V. Iebba, *Physical Review Letters* **106**, 038101 (2011).
- [16] M. Morse, A. Huang, G. Li, M. R. Maxey, and J. X. Tang, *Biophysical Journal* **105**, 21 (2013).
- [17] K. Ishimoto and E. A. Gaffney, *Physical Review E* **88**, 062702 (2013).
- [18] L. Cisneros, C. Dombrowski, R. E. Goldstein, and J. O. Kessler, *Physical Review E* **73**, 030901 (2006).
- [19] A. P. Berke, L. Turner, H. C. Berg, and E. Lauga, *Physical Review Letters* **101**, 038102 (2008).
- [20] G. Li and J. X. Tang, *Physical Review Letters* **103**, 078101 (2009).
- [21] G. Li, J. Besson, L. Nisimova, D. Munger, P. Mahautmr, J. X. Tang, M. R. Maxey, and Y. V. Brun, *Physical Review E* **84**, 041932 (2011).
- [22] M. Molaei, M. Barry, R. Stocker, and J. Sheng, *Physical Review Letters* **113**, 068103 (2014).
- [23] K. Schaar, A. Zöttl, and H. Stark, *Physical Review Letters* **115**, 038101 (2015).
- [24] S. E. Spagnolie and E. Lauga, *Journal of Fluid Mechanics* **700**, 105 (2012).
- [25] S. E. Spagnolie, G. R. Moreno-Flores, D. Bartolo, and E. Lauga, *Soft Matter* **11**, 3396 (2015).
- [26] N. Desai, V. Shaik, and A. M. Ardekani, *Soft Matter* (2017), 10.1039/C7SM01615H.
- [27] G. O’Toole, H. B. Kaplan, and R. Kolter, *Annual Review of Microbiology* **54**, 49 (2000).
- [28] T. Danhorn and C. Fuqua, *Annual Review of Microbiology* **61**, 401 (2007).
- [29] A. Karimi, D. Karim, A. Kumar, and A. M. Ardekani, *Lab Chip* **15**, 23 (2015).
- [30] G. A. Jackson, *Limnology and Oceanography* **32**, 1253 (1987).
- [31] G. A. Jackson, *Limnology and Oceanography* **34**, 514 (1989).
- [32] R. Bearon and T. J. Pedley, *Bulletin of Mathematical Biology* **62**, 775 (2000).
- [33] T. Kiorboe and G. A. Jackson, *Limnology and Oceanography* **46**, 1309 (2001).
- [34] T. Kiorboe, H.-P. Grossart, H. Ploug, and K. Tang, *Applied and Environmental Microbiology* **68**, 3996 (2002).
- [35] R. N. Bearon, *Bulletin of Mathematical Biology* **69**, 417 (2007).
- [36] J. T. Locsei and T. J. Pedley, *Microbial Ecology* **58**, 63 (2009).
- [37] R. Stocker, *Science* **338**, 628 (2012).
- [38] R. Stocker and J. R. Seymour, *Microbiology and Molecular Biology Reviews* **76**, 792 (2012).
- [39] E. Lushi, R. E. Goldstein, and M. J. Shelley, *Physical Review E* **86**, 040902 (2012).
- [40] E. Lushi, *Physical Review E* **94**, 022414 (2016).
- [41] D. Takagi, J. Palacci, A. B. Braunschweig, M. J. Shelley, and J. Zhang, *Soft Matter* **10**, 1784 (2014).
- [42] K. Drescher, J. Dunkel, L. H. Cisneros, S. Ganguly, and R. E. Goldstein, *Proceedings of the National Academy of Sciences* **108**, 10940 (2011).
- [43] L. G. Leal, *Advanced Transport Phenomena* (Cambridge University Press, Cambridge, 2007).
- [44] G. M. Barbara and J. G. Mitchell, *FEMS Microbiology Ecology* **44**, 79 (2003).
- [45] D. Lopez and E. Lauga, *Physics of Fluids* **26**, 071902 (2014).
- [46] V. A. Shaik and A. M. Ardekani, *Journal of Fluid Mechanics* **824**, 42 (2017).
- [47] S. Kim and S. Karrila, *Microhydrodynamics: Principles and Selected Applications* (Butterworth-Heinemann, Boston, 1991).
- [48] V. A. Shaik and A. M. Ardekani, *Physical Review Fluids* **2**, 113606 (2017).
- [49] I. M. Head, D. M. Jones, and W. F. M. Röling, *Nature Reviews Microbiology* **4**, 173 (2006).
- [50] L. Turner, W. S. Ryu, and H. C. Berg, *Journal of Bacteriology* **182**, 2793 (2000).
- [51] M. J. Kim, M. J. Kim, J. C. Bird, J. Park, T. R. Powers, and K. S. Breuer, *Experiments in Fluids* **37**, 782 (2004).
- [52] N. C. Darnton and H. C. Berg, *Biophysical Journal* **92**, 2230 (2007).
- [53] J. Elgeti, R. G. Winkler, and G. Gompper, *Reports on Progress in Physics* **78**, 056601 (2015).
- [54] C. Bechinger, R. Di Leonardo, H. Löwen, C. Reichhardt, G. Volpe, and G. Volpe, *Reviews of Modern Physics* **88**, 045006 (2016).
- [55] P. D. Cobb and J. E. Butler, *The Journal of Chemical Physics* **123**, 054908 (2005).
- [56] M. De Corato, F. Greco, G. D’Avino, and P. L. Maffettone, *The Journal of Chemical Physics* **142**, 194901 (2015).
- [57] P. D. Frymier, R. M. Ford, and P. T. Cummings, *AIChE Journal* **40**, 704 (1994).
- [58] K. Duffy, P. Cummings, and R. Ford, *Biophysical Journal* **68**, 800 (1995).
- [59] M. Abramowitz and I. A. Stegun, *Handbook of Mathematical Functions with Formulas, Graphs, and Mathematical Tables*, 9th ed. (Dover, New York, NY, 1972).
- [60] K. C. Chen, R. M. Ford, and P. T. Cummings, *Journal of Mathematical Biology* **47**, 518 (2003).
- [61] D. Saintillan, *Annual Review of Fluid Mechanics* **50**, anurev (2018).
- [62] T. V. Kasyap and D. L. Koch, *Journal of Fluid Mechanics* **741**, 619 (2014).
- [63] P. J. Brandvik, Ø. Johansen, F. Leirvik, U. Farooq, and P. S. Daling, *Marine Pollution Bulletin* **73**, 319 (2013).
- [64] Ø. Johansen, P. J. Brandvik, and U. Farooq, *Marine Pollution Bulletin* **73**, 327 (2013).
- [65] E. W. North, E. E. Adams, A. E. Thessen, Z. Schlag, R. He, S. A. Socolofsky, S. M. Masutani, and S. D. Peckham, *Environmental Research Letters* **10**, 024016 (2015).
- [66] E. L. Cussler, *Diffusion: Mass Transfer in Fluid Systems*, 2nd ed. (Cambridge University Press, New York, NY, 1997).
- [67] G. A. Jackson, *Journal of Experimental Biology* **215**, 1017 (2012).
- [68] R. C. Macnab and D. E. Koshland Jr., *Proceedings of the National Academy of Sciences* **69**, 2509 (1972).
- [69] E. A. Codling, M. J. Plank, and S. Benhamou, *Journal of The Royal Society Interface* **5**, 813 (2008).
- [70] M. J. Tindall, S. L. Porter, P. K. Maini, G. Gaglia, and J. P. Armitage, *Bulletin of Mathematical Biology* **70**, 1525 (2008).
- [71] K. Son, F. Menolascina, and R. Stocker, *Proceedings of the National Academy of Sciences* **113**, 8624 (2016).
- [72] M. Molaei and J. Sheng, *Scientific Reports* **6**, 35290 (2016).

- [73] G. Subramanian, D. L. Koch, and S. R. Fitzgibbon, *Physics of Fluids* **23**, 041901 (2011).
- [74] G. Perkins and R. Jones, *Physica A: Statistical Mechanics and its Applications* **189**, 447 (1992).
- [75] B. Cichocki and R. Jones, *Physica A: Statistical Mechanics and its Applications* **258**, 273 (1998).
- [76] R. B. Jones, *The Journal of Chemical Physics* **123**, 164705 (2005).
- [77] J. M. Al-Besharah, O. A. Salman, and S. A. Akashah, *Industrial & Engineering Chemistry Research* **26**, 2445 (1987).